Computer simulation of wetting and drying of spherical particulates at a liquid–vapor interface

Fernando Bresme and Nicholas Quirke

Citation: The Journal of Chemical Physics **110**, 3536 (1999); doi: 10.1063/1.478221
View online: http://dx.doi.org/10.1063/1.478221
View Table of Contents: http://scitation.aip.org/content/aip/journal/jcp/110/7?ver=pdfcov
Published by the AIP Publishing

Computer simulation of wetting and drying of spherical particulates at a liquid–vapor interface

Fernando Bresme and Nicholas Quirke[a)]
Department of Chemistry, University of Wales at Bangor, Bangor, Gwynedd LL57 2UW, United Kingdom and Department of Chemistry, Imperial College of Science, Technology and Medicine, Exhibition Road, London SW7 2AY, United Kingdom

(Received 6 August 1998; accepted 10 November 1998)

We investigate the behavior of model particulates of nanometer size at a liquid–vapor interface. The particulate undergoes wetting and drying transitions, defined by its penetration in the liquid and vapor phases, respectively. We have analyzed the dependence of the wetting and drying of this particulate in terms of the fluid–particulate interaction strength and range, and particulate radius. We have also considered the limit of a particulate of infinite radius, where the model becomes equivalent to a system consisting of a fluid in contact with a planar wall. We have explored the effect that the curvature of the substrate has on the wetting and drying transitions. The wetting transition in our model is very sensitive to the size of the particulate (curvature of the substrate), whereas the drying transition is essentially independent. Small particulates are less stable at the liquid–vapor interface than larger ones, and they exhibit enhanced solubility. Our results suggest that curved surfaces can be wetted more easily than planar substrates. As expected, long range attractive interactions enhance wetting, but our simulations show that this enhancement is larger in curved surfaces than in planar ones. The description of the wetting behavior of the particulates using Young's equation breaks down for the smallest particulates considered. We have computed the line tensions for our model using a methodology introduced previously [F. Bresme and N. Quirke, Phys. Rev. Lett. **80**, 3791 (1998)]. They are found to be negative and of the order of $\approx 10^{-12}$ N. © *1999 American Institute of Physics.*
[S0021-9606(99)50407-8]

I. INTRODUCTION

Wetting phenomena have attracted considerable interest in the last few years.[1] Part of this interest is motivated by applications to industrial problems including, for example, foams, lubrication, and adhesion, but the range of potential applications is clearly much wider. Computer simulations have proved helpful in extending our understanding of the microscopic mechanisms of wetting. Most simulation studies have focused on fluids adsorbed on a planar solid substrate.[2–9] From this work it is known that a change of the fluid–substrate interaction strength can induce drying and wetting transitions. Such modifications mimic experiments where the properties of the surface of the substrate can be altered by chemical treatment.[10] Simulation studies have made it possible to test the validity of Young's equation as a description of the wetting behavior of a fluid adsorbed on a planar substrate[4] as well as indicating the order of wetting and drying transitions.[4,5,9] These studies show that the wetting transition is first order, whereas drying is weakly first order or second order. Density functional theories predict drying transitions of second order.[11]

Adsorption on curved surfaces has attracted less attention. However the study of curved surfaces can be relevant to our understanding of wetting on real substrates which generally present some degree of roughness and therefore deviate from an ideal planar geometry. Substrate curvature influences processes such as capillary condensation or solubility and is important in nonequilibrium phenomena such as nucleation.[12] Thus far the adsorption of simple fluids on a spherical surface has been considered using density functional approaches (see for instance Ref. 13 and references therein, and Ref. 14). As a consequence of the curvature, the adsorbed wetting layer exhibits a finite thickness, in contrast to a planar substrate, where this layer can become macroscopic. In addition, adsorption on small spherical substrates is subject to finite size effects which affect the location of the wetting transition. The wetting temperature depends on the size of the spherical substrate, increasing as the size of the substrate diminishes. This behavior might be of relevance in colloidal chemistry; it has been suggested on theoretical grounds that the wetting of colloidal particles enhances the aggregation process.[15]

Spherical substrates such as colloidal particulates are important in several industrial processes. Particulates of nanometer size such as ''overbased detergents'' are used as additives in petrochemical industry.[16,17] Dispersions of small particulates are relevant in foams and emulsions. It is believed that the effectiveness of the particulates as antifoam agents depends on their ability to enter liquid/vapor and

[a)]Author to whom correspondence should be addressed at Dept. of Chemistry, Imperial College of Science, Technology and Medicine, Exhibition Road, London; electronic mail: n.quirke@ic.ac.uk

liquid/liquid interfaces. Depending on their hydrophobicity the particulates may enter one phase or the other, i.e., they may undergo drying or wetting transitions. These are the kind of systems we consider in this article. We study a model consisting of a particulate at a liquid–vapor interface. We will see that the wetting behavior of this particulate depends on the particulate–fluid interaction strength and/or range, and also on the size of the particulate. In this respect computer simulations can help us to understand the microscopic phenomena that influence the stability of particulates at interfaces.

One important feature of a small spherical substrate in a liquid–vapor interface, is that the interface formed by the line where the three phases meet (liquid–vapor–particulate) has a significant curvature. Under these conditions it is expected that the line tension will influence the wetting behavior of the system. The line tension[1,18,19] is a property characteristic of the three phase equilibrium, in the same way that the surface tension is of the equilibrium between two phases. It is known from theoretical analysis that the line tension can have considerable influence on the wetting transition of some systems,[20,21] and therefore must be included as a correction in a more general treatment.[22,23] The line tension will therefore be relevant to phenomena involving wetting and curved surfaces such as those mentioned above.[24–28] Despite its importance there is no consensus on the magnitude or sign of the line tensions of many systems,[29] and a wide range of values can be found in the literature.[16,30–35]

Recently we have reported computer simulation results for the wetting behavior and line tensions of spherical particulates at a liquid–vapor interface obtained using a novel methodology.[36] Our results suggest that the line tension plays an important role in determining the location of the wetting transition of small spherical substrates. In this work we extend the study reported previously and we analyze in detail the wetting and drying behavior of the particulate as a function of size, fluid–particulate interaction strength, and potential range. We compare the results for nanoparticulates with those of a particulate of infinite radius, i.e., the planar wall limit. These studies enable us to draw a diagram of the wetting and drying boundaries of the particulate in terms of the particulate size and the fluid–substrate interaction strength. The implications for the behavior of particulates at interfaces; their stability, and the influence of curvature on the wetting and drying transitions are discussed.

In addition we analyze Young's equation in the context of the prediction of the contact angles of the particulate at the liquid–vapor interface. We will see that this approximation is not accurate for the wetting of very small particulates, though it gives reasonable predictions for the larger particulates considered in this work. We also present results on the line tension of our system and we discuss different routes used to estimate this property.

II. METHODOLOGY

A. Model potential and simulation details

We consider a spherical particulate (p) of radius R at a planar liquid (l)–vapor (v) interface (see Fig. 1). The location of the particulate in the interface can be described in terms of the contact angle θ, which is the angle that the particulate makes with the surface (see Fig. 1). Alternatively we can use the depth of immersion of the particulate in the liquid h, which is related to the contact angle through $\cos\theta = h/R - 1$. In the simulations we calculate d, where $d = R - h$ and represents the average distance between the particulate and the equimolar dividing surface taken at the liquid–vapor interface, the latter computed as explained below. Following previous work[36] we have chosen a potential model based on the Lennard-Jones/spline (LJ/s) potential:[37,38]

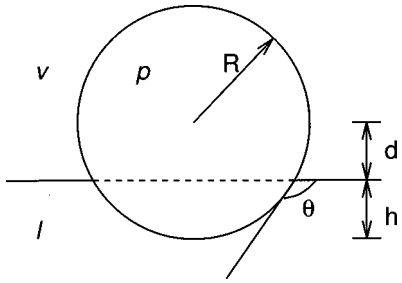

FIG. 1. Illustration of a particulate at the liquid–vapor interface. For definitions see text.

$$U_{ij}(r,s) = \begin{cases} 4\epsilon_{ij}\left[\left(\dfrac{\sigma_f}{r-s}\right)^{12} - \left(\dfrac{\sigma_f}{r-s}\right)^{6}\right] & \text{if } 0 < r-s < r_{s,ij} \\ a_{ij}(r-s-r_{c,ij})^2 + b_{ij}(r-s-r_{c,ij})^3 & \\ \quad \text{if } r_{s,ij} < r-s < r_{c,ij}, & \\ 0 \quad \text{if } r_{c,ij} < r-s & \end{cases} \tag{2.1}$$

where r is the distance between particles, σ_f is the diameter of the fluid particles, i.e., the particles which form the liquid–vapor interface, ϵ_{ij} represents the potential depth for interactions between species i and j, and $s = (\sigma_p - \sigma_f)/2$, where $\sigma_p = 2R$ is the diameter of the particulate. The remaining variables are given by $r_{s,ij} = (26/7)^{1/6}\sigma_f$, $r_{c,ij} = (67/48) r_{s,ij}$, $a_{ij} = -(24\,192/3211)(\epsilon_{ij}/r_{s,ij}^2)$, and $b_{ij} = -(387\,072/61\,009)(\epsilon_{ij}/r_{s,ij}^3)$. We define the reduced temperature $T^* = k_B T/\epsilon_{\rm ff}$, where k_B the Boltzmann constant, and the reduced density, $\rho^* = N\sigma_f^3/V$, where N is the total number of particles filling a volume V. Figure 2 sketches the

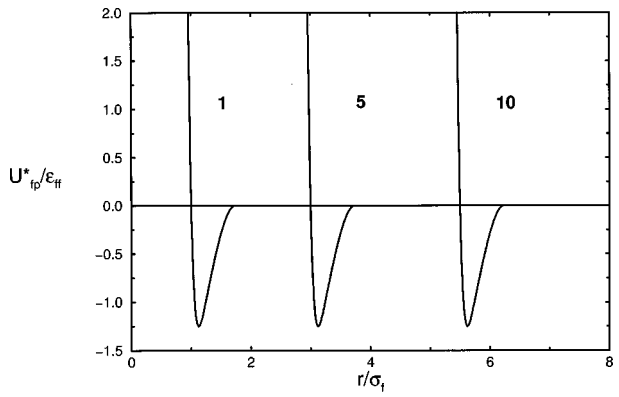

FIG. 2. Fluid–particulate potential for $\epsilon_{\rm fp} = 1.25\epsilon_{\rm ff}$, and $\sigma_p = 1$,5, and $10\sigma_f$.

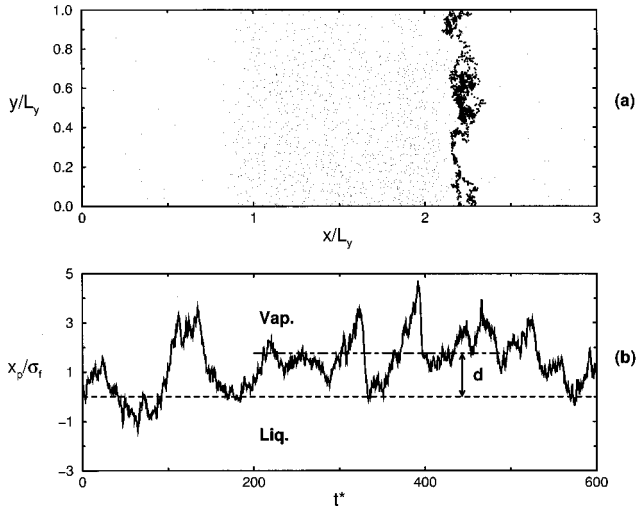

FIG. 3. (a) Snapshot of a typical liquid–vapor interface. Dots represent fluid particles and black circles the trajectory followed by a particulate of size $\sigma_p=5\sigma_f$, with $\epsilon_{\rm fp}=1.1\epsilon_{\rm ff}$. (b) x coordinate of the trajectory represented in (a), referred to the equimolar dividing surface. The dash dotted line represents a time average employed to calculate the distance of the particulate to the interface, i.e., d.

potential model for $\epsilon_{\rm fp}/\epsilon_{\rm ff}=1.25$ as a function of the particulate diameter. The potential has a finite range and for the particulate–fluid interactions it is independent of the size of the particulate (see Fig. 2), even for an infinite radius, where the particulate represents a planar structureless wall. We will make use of this fact in the paper to compare the wetting behavior of finite particulates at the liquid–vapor interface with that of a fluid in contact with a wall.

Using the model defined in Eq. (2.1) we have performed molecular dynamics[39] simulations of the particulate at the interface in the canonical ensemble. We have employed a constraint method and the dynamics was generated using a modified leap-from algorithm.[40] Figure 3(a) illustrates a typical system considered in this work, consisting of a liquid slab located in the middle of the box surrounded by the coexisting vapor phase. Periodic boundary conditions are imposed in all three directions. The simulation box is prismatic with lengths in the ratio $\{x,y,z\}=\{3,1,1\}$ [see Fig. 3(a)]. The time step was set to $\delta t^*=\delta t\sqrt{\epsilon_{\rm ff}/(m\sigma_f^2)}=0.005$, where m represents the mass of both the fluid particles and the particulate. The number of particles varied from 4000 to 13 500 for small diameters $\sigma_p=1-5\sigma_f$, up to $N=23\,328$ for the larger particulates $\sigma_p=7$, $10\sigma_f$. These system sizes are large enough to consider that the particulate is at infinite dilution, and therefore the influence of finite size effects on the measured contact angles is expected to be negligible. Indeed the perturbation induced by the particulate on the fluid was restricted to a small volume of the simulation box. For distances far from the particulate, $3-4\sigma_f$, the coexistence densities of the liquid–vapor interface are equal, inside statistical uncertainties, to the coexistence densities obtained from a simulation of the liquid–vapor interface alone. All the simulations were performed using the cell linked method algorithm[40] in order to improve the efficiency of the calculations.

The particulate was created in an equilibrium liquid–vapor configuration by choosing one of the fluid particles near the interface and increasing its size in a stepwise fashion to the desired radius. This was followed by an equilibration of the system lasting $5-10\times10^4$ time steps, and a production phase of $1-2\times10^5$ time steps. In the case of larger particulates the production run was longer, up to $3-5\times10^5$. In Fig. 3(a) we have shown the projection, on the xy plane, of the trajectory of a particulate of size $\sigma_p/\sigma_f=5$ at the liquid–vapor interface. The particulate diffuses freely in the yz plane, but its movement is constrained in a well defined layer in the x direction. Figure 3(b) depicts the x coordinate of the trajectory mentioned above as a function of time, and referred to as the equimolar dividing surface of the liquid–vapor interface. The time average of this coordinate gives us the average position of the particulate with respect to the interface, i.e., the variable we have called d. The contact angle is computed readily from $\cos\theta=-d/R$. The equimolar dividing surface was calculated by taking averages of the density profile, obtained by dividing the simulation cell in layers parallel to the interface, and calculating the average density in each layer. All these profiles were fitted to the expression:[18]

$$\rho(x)=\frac{1}{2}(\rho_l+\rho_v)-\frac{1}{2}(\rho_l-\rho_v)\tanh\left(\frac{x-x_e}{w}\right), \tag{2.2}$$

where ρ_l and ρ_v represent the liquid and vapor coexistence densities, x_e represents the location of the equimolar dividing surface, and w is a measurement of the thickness of the interface.

We made some preliminary calculations to evaluate the influence of the simulation length on the values of the contact angle. For instance for $\sigma_p/\sigma_f=5$ and $\epsilon_{\rm fp}/\epsilon_{\rm ff}=1.25$, for a simulation comprising 5×10^5 time steps we obtained $\cos\theta=-0.11\pm0.14$, as compared with $\cos\theta=-0.10\pm0.33$ using 2×10^5 time steps. For other systems we obtained similar agreement: for $\sigma_p/\sigma_f=7.0$ and $\epsilon_{\rm fp}/\epsilon_{\rm ff}=1.75$ we have: $\cos\theta=0.78\pm0.1$ for 6×10^5 time steps, and $\cos\theta=0.82\pm0.15$ for 3×10^5 time steps. Therefore, for the simulation times considered here, it follows that an increase in the length of the simulation does not change significantly the value of the contact angles.

We also consider the wetting and drying transitions of a particulate of infinite size, i.e., the wetting of a fluid on a planar substrate. Our model comprises a liquid in coexistence with its vapor, enclosed in the x direction by two walls. The fluid particles interact with the walls through the potential described above by expression (2.1) where $(r-s)$ represents, in this case, the distance of particulate–wall in the x direction. The samples consisted of 6912 fluid particles in a simulation box whose length in the direction normal to the walls (x) is twice as large as that in the parallel directions (y,z). The sectional area of our system is $483\sigma_f^2$. The simulations were performed in the microcanonical ensemble and the system temperature was scaled each 100 time steps in order to maintain the desired value. Local properties such as density, pressure tensor, and temperature, were computed in layers parallel to the walls and averages were obtained in each layer. The simulations comprise typically $3-5\times10^4$

time steps of equilibration and 5×10^4 of production, the time step being $\delta t^*=0.005$.

B. Computation of the line and surface tensions

The excess free energy associated with the three phase system: liquid–vapor–particulate (i.e., the line tension) was calculated using the methodology introduced in a previous publication.[36]

The free energy of the particulate in the planar surface with respect to the planar liquid–vapor interface is defined as:[21]

$$F^s=2\pi R^2\Big(\gamma_{\rm pl}(1+\cos\theta)+\gamma_{\rm pv}(1-\cos\theta)-0.5\gamma_{\rm lv}\sin^2\theta+\frac{\tau\sin\theta}{R}\Big), \tag{2.3}$$

where $\gamma_{\alpha\beta}$ represents the surface tension between phases α and β, τ is the line tension and, θ stands for the contact angle. To estimate τ from Eq. (2.3), the contact angle and the surface tensions $\gamma_{\rm pl}$, $\gamma_{\rm pv}$, and $\gamma_{\rm lv}$ are required. These were obtained by considering the work done on the system to reversibly and isothermally increase/decrease the radius of the spherical particulate by an amount dR. The free energy associated with this process is defined as

$$dF=(8\pi R_s\gamma_{\alpha\beta})dR_s+(4\pi R_s^2P_{\rm out})dR_s, \tag{2.4}$$

where R_s represents the radius of the surface of tension that separates the two phases.[18] We have considered $R_s=R$, i.e., equal to the radius of the particulate. This choice produces surface tensions which are consistent with the corresponding values for a particulate of infinite radius, i.e., the wall–fluid system. Note that in the latter case the surface tensions were calculated by an independent route (from the pressure tensor).

The pressure term $P_{\rm out}$ in Eq. (2.4) represents the fluid pressure against which the particulate does work. This corresponds to the bulk pressure of the fluid surrounding the particulate, and given we are considering a liquid phase in equilibrium with its vapor, this pressure term is equal to the saturation pressure.

Provided the change in the free energy in Eq. (2.4) is small ($<k_BT$), it can be estimated from computer simulations in the canonical ensemble as follows. The free energy difference ΔF between two systems, differing only in the radius of an atom by an amount ΔR, is given by

$$\begin{aligned}dF\equiv\Delta F&=F_{R'}(N,V,T)-F_R(N,V,T)\\&=-k_BT\ln\frac{Q'(N,V,T)}{Q(N,V,T)}\\\frac{Q'(N,V,T)}{Q(N,V,T)}&=\frac{\int\exp[-\beta U(q,R')]dq}{\int\exp[-\beta U(q,R)]dq}\\&=\langle\exp\{-\beta[U(R')-U(R)]\}\rangle_R,\end{aligned} \tag{2.5}$$

where $U(R')$ and $U(R)$ are the potential energies of ''perturbed'', i.e., $R'=R\pm\Delta R$, and reference states R, and the subindex R in Eq. (2.5) denotes that the average is taken over the reference state. To calculate the surface tensions $\gamma_{\rm pv}$ and $\gamma_{\rm pl}$, we performed molecular dynamics simulations of a system consisting of the particulate and the fluid, the latter being at the coexistence pressure. The particulate changes the density of the fluid slightly. To correct this we adjusted the overall density of the system in such a way that the bulk density of the fluid with respect to the particulate, defined as the mean value of the density profile at large separations, was close to the fluid coexistence density. With this adjustment the fluid bulk pressure is equal, within statistical error, to the value at saturation. In the calculation of the liquid–particulate surface tensions, the number of fluid particles was $N=13\,500$ for relatively small particulates, $\sigma_p/\sigma_f=1-5$, and $N=23\,328$ for the larger ones, $\sigma_p/\sigma_f=7,10$. For the vapor–particulate surface tensions we employed $N=1372$ and $N=5324$ for particulate sizes in the range $\sigma_p/\sigma_f=1-4$ and 5–10, respectively. The simulations involved around 10^5 time steps for liquid–particulate systems and 5×10^5 time steps for vapor–particulate calculations.

TABLE I. Dependence of the liquid–particulate surface tension with the variable ΔR. $\sigma_p/\sigma_f=5$ and $\epsilon_{\rm p}/\epsilon_{\rm ff}=1.25$. Numbers in parenthesis represent the error associated to the data.

$\Delta R/\sigma_f$	γ^*
0.0025	0.0546(40)
0.0050	0.0575(80)
0.0075	0.0513(80)

The convergence of the ensemble average given in Eq. (2.5) depends on the choice of ΔR. We used values in the range, $0.0025-0.025\sigma_f$, the smaller ones for the particulate–liquid, and the larger for the particulate–vapor surface tensions. Table I illustrates the effect of ΔR on the liquid–particulate surface tension of a representative system, $\sigma_p/\sigma_f=5$ and $\epsilon_{\rm fp}/\epsilon_{\rm ff}=1.25$. The results do not show a systematic dependence on ΔR, and the surface tensions agree within the statistical error.

The liquid–vapor surface tension $\gamma_{\rm lv}$, of the planar interface was computed using the mechanical definition,[18] evaluating the integral over the interface of the difference between the normal P_N and tangential P_T components of the pressure tensor:

$$\gamma_{\rm lv}=\int_{x_l}^{x_v}[P_N(x)-P_T(x)]dx, \tag{2.6}$$

where x_l and x_v correspond to arbitrary positions in the liquid and vapor bulk phases, respectively. The local components of the pressure tensor were computed as follows. The system was divided into n_l layers of thickness n_l/L_x and volume $V_l=L_xL_yL_z/n_l$, parallel to the interface. The local components of the pressure tensor are given by[18]

$$P_N(l)=\langle\rho(l)\rangle k_BT-\frac{1}{V_l}\Big\langle\sum_{(i,j)}^{(l)}\frac{x_{ij}^2}{r_{ij}}\frac{dU}{r_{ij}}\Big\rangle, \tag{2.7}$$

$$P_T(l)=\langle\rho(l)\rangle k_BT-\frac{1}{2V_l}\Big\langle\sum_{(i,j)}^{(l)}\frac{y_{ij}^2+z_{ij}^2}{r_{ij}}\frac{dU}{r_{ij}}\Big\rangle, \tag{2.8}$$

where the brackets denote an ensemble average, and the sum $\Sigma_{ij}^{(l)}$ runs over all pairs of particles (i,j) of which at least one of these particles is in layer l. When two particles are in different layers, we add half of the contribution of the second term in Eqs. (2.7) and (2.8), to the layer where particle i resides, and the other half to the corresponding layer for particle j. If the two particles are in the same layer, we add the overall contribution. This procedure does not have any influence on the value of the surface tension $\gamma_{\rm lv}$, given this quantity is the result of the integral of $(P_N - P_T)$, and this is independent of the distribution of the different contributions over the layers.

The surface tensions in the wall–fluid system were calculated using the same procedure, but in this case we add the contribution from the external field due to the wall[4]

$$\gamma_{\rm wf} = \frac{1}{A}\int_A dy\, dz \int_0^\infty \left(p_N(\mathbf{r}) - p_T(\mathbf{r}) - \rho(\mathbf{r}) x \frac{\partial U_{\rm wf}(\mathbf{r})}{\partial x} \right) dx, \tag{2.9}$$

where the wall is located at $x=0$, $U_{\rm wf}$ represents the wall–fluid interaction as given by Eq. (2.1), and A is the area of the wall.

In addition to the surface tensions, the calculation of the line tension requires the free energy of the particulate at the liquid–vapor interface F^s [see Eq. (2.3)]. By analogy with Eq. (2.4) we employ the following expression:

$$dF = \{4\pi R[\,\gamma_{\rm pl}(1+\cos\theta) + \gamma_{\rm pv}(1-\cos\theta) - 0.5\gamma_{\rm lv}\sin^2\theta] + (2\pi\tau\sin\theta)\}dR + (4\pi R^2 P_{\rm out})dR, \tag{2.10}$$

where the first term in square brackets represents the force due to the surface tension and line tension against which the particulate does work. The pressure term $P_{\rm out}$ is the saturation pressure as before. The free energy $dF \equiv \Delta F$ was obtained employing the methodology explained above for the calculation of the surface tensions. In this case ΔR was in the interval $0.005-0.025\sigma_f$. The free energy ΔF was obtained as an ensemble average over a system consisting of a liquid–vapor interface and a particulate located in the interface [see Fig. 3(a)]. As discussed in Sec. II the particulate diffuses in a well defined layer and this facilitates the calculation of ΔF. Once free energy, surface tensions, and contact angles are known, τ can be obtained from Eq. (2.10).

III. RESULTS AND DISCUSSION

A. Contact angles and the wetting–drying transition

In the following we analyze the wetting properties of a particulate at a liquid–vapor interface in terms both of the particulate–fluid interaction strength and the particulate diameter. As in previous work[36] we have considered a single thermodynamic state $T^*=0.75$. By comparison the critical temperature of the LJ/s model obtained from simulations of the liquid–vapor interface is $T_c^* \approx 0.91$. The coexistence densities for this state are $\rho_l^* = 0.675 \pm 0.003$ and $\rho_v^* = 0.046 \pm 0.001$, and the saturation pressure is $P^* = P\sigma_f^3/\epsilon_{\rm ff} = 0.026 \pm 0.007$. The surface tension of the planar liquid–vapor interface at $T^*=0.75$ is $\gamma_{\rm lv}^* = \gamma_{\rm lv}\sigma_f^2/\epsilon_{\rm ff} = 0.165 \pm 0.009$.

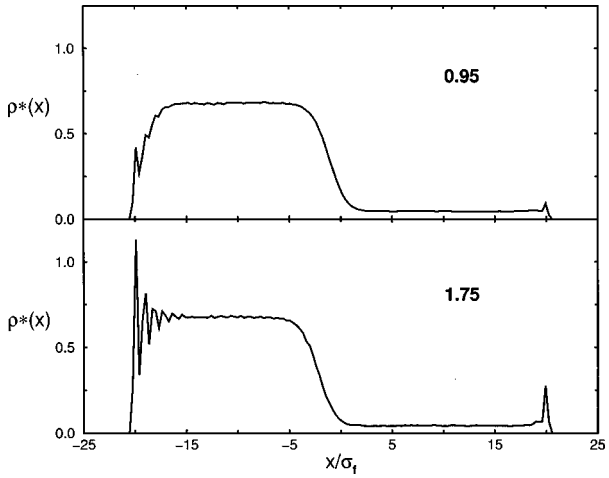

FIG. 4. Density profile of a wall–fluid system showing: (a) partially dry state ($\cos\theta<0$) and (b) partially wet states ($\cos\theta>0$).

For a particulate of infinite size our model represents a system consisting of a wall in contact with a liquid which is in coexistence with its vapor. It has been shown that the variation of the substrate–fluid interaction strength changes the wetting properties of the system, and eventually can drive wetting and drying transitions.[2–5,41] We have studied these transitions evaluating the contact angle, obtained from the wall–liquid $\gamma_{\rm wl}$ and wall–vapor $\gamma_{\rm wv}$ surface tensions using Young's equation:

$$\cos\theta = \frac{\gamma_{\rm wv} - \gamma_{\rm wl}}{\gamma_{\rm lv}}. \tag{3.1}$$

This expression is very accurate when used to predict the contact angle in the case of wall–fluid systems.[4] The surface tensions were calculated using a system consisting of a liquid in equilibrium with its vapor, which is enclosed in the direction normal to the interface by two walls. Figure 4 depicts typical asymmetric density profiles for partially wet ($\cos\theta>0$) and partially dry ($\cos\theta<0$) states of this system. The wall induces a structure in the fluid which depends strongly on the wall–fluid interaction strength $\epsilon_{\rm wf}/\epsilon_{\rm ff}$. The vapor density profile is characterized by a single peak and approaches the bulk density in a few molecular diameters. The external field due to the wall induces a marked layering in the liquid phase.

Table II compiles surface tension data as well as contact angles predicted by Young's equation, and Fig. 5 depicts the dependence of these contact angles on the interaction strength. We have used for the liquid–vapor surface tension the value reported previously,[36] i.e., $\gamma_{\rm lv}^* = 0.165 \pm 0.009$. There is no systematic dependence of the (lv) surface tension on the wall interaction strength. The surface tension obtained from the wall–fluid system by averaging over the different interaction strengths is 0.165. The coexistence densities for the wall–fluid system were the same within the statistical error as those obtained from the simulation of a free liquid–vapor interface. The wetting and drying transitions are determined by the interaction strengths for which the contact angle has the values $\cos\theta=+1$ and $\cos\theta=-1$, respectively. From our results we locate the wetting transition at $\epsilon_{\rm wf}/\epsilon_{\rm ff}$

TABLE II. Wall–fluid surface tensions and contact angles as a function of wall–fluid interaction strength. The contact angles were obtained from Young's equation using $\gamma_{lv}^{*}=0.165\pm0.009$.

$\epsilon_{wf}/\epsilon_{ff}$	γ_{wv}^{*}	γ_{wt}^{*}	γ_{lv}^{*}	$\cos\theta$
2.25	−0.112(15)	−0.287(7)	0.174(10)	1.06(12)
2.20	−0.118(6)	−0.259(40)	0.165(18)	0.86(25)
2.15	−0.112(6)	−0.234(30)	0.179(20)	0.74(15)
2.10	−0.108(6)	−0.219(20)	0.164(20)	0.68(10)
1.90	−0.054(4)	−0.130(20)	0.169(20)	0.46(14)
1.75	−0.047(9)	−0.091(15)	0.161(10)	0.27(10)
1.60	−0.034(6)	−0.030(20)	0.159(17)	−0.02(1)
1.50	−0.024(6)	0.005(20)	0.163(14)	−0.17(8)
1.25	−0.0064(30)	0.090(7)	0.153(5)	−0.58(3)
1.05	0.0031(10)	0.138(5)	0.174(25)	−0.76(12)
1.00	0.0055(20)	0.156(10)	0.161(20)	−0.92(8)
0.95	0.0084(20)	0.149(10)	0.171(23)	−0.85(8)
0.90	0.0088(10)	0.165(20)	0.160(25)	−0.95(12)
0.85	0.0108(10)	0.164(10)	0.167(17)	−0.93(9)
0.80	0.0106(10)	0.178(25)	0.146(20)	−1.01(20)
0.70	0.0152(20)	0.180(5)	0.157(9)	−1.00(3)
2.0[a]	−0.109(4)	−0.267(18)	0.163(14)	0.96(9)
1.5[a]	−0.0247(50)	−0.040(20)	0.162(24)	0.09(10)
1.25[a]	−0.0087(41)	0.0367(31)	0.163(10)	−0.27(17)
1.0[a]	0.001(3)	0.092(25)	0.169(24)	−0.55(15)

[a]The wall–fluid interaction is of the type Lennard-Jones truncated at $r=3.8\sigma_f$.

$=2.28\pm0.05$, and drying appears at $\epsilon_{wf}/\epsilon_{ff}=0.75\pm0.10$. The variation of the contact angle with the interaction strength suggest that the wetting transition is first order, whereas the drying transition is likely second order or weakly first order. These observations are in agreement with results reported by different authors for a similar wall–fluid system.[3]

In a previous letter[36] we have presented some preliminary results for the wetting of particulates at a liquid–vapor interface. There we have shown that the contact angles predicted by Young's equation for small particulates are in poor agreement with the data obtained for this quantity by direct observation in a computer simulation of the three phase system; particulate–liquid–vapor. In the present work we have

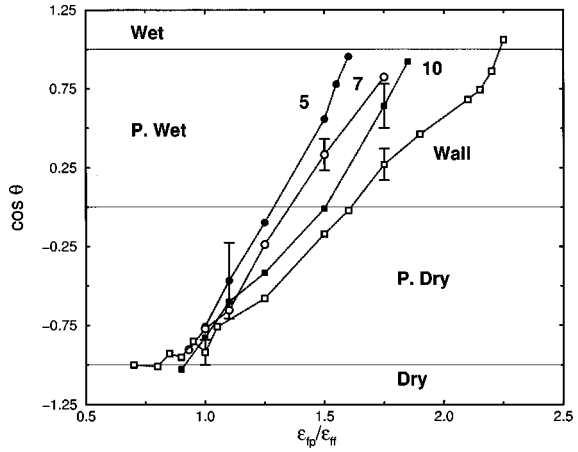

FIG. 5. Contact angles as a function of particulate–fluid interaction strength for several particulate sizes, 5, 7, and $10\sigma_f$, and the infinite limit, i.e., the wall–fluid system. See Tables II and III for numerical values.

TABLE III. Contact angles for several particulate sizes as a function of interaction strength.

σ_p/σ_f	$\epsilon_{fp}/\epsilon_{ff}$	$\cos\theta$
5	1.00	−0.76(19)
	1.10	−0.47(24)
	1.25	−0.10(33)
	1.50	0.56(11)
	1.55	0.78(36)
	1.60	0.95(26)
7	0.93	−0.90(10)
	1.00	−0.77(10)
	1.10	−0.65(10)
	1.25	−0.24(15)
	1.50	0.33(10)
	1.75	0.82(15)
10	0.90	−1.03(17)
	1.00	−0.83(5)
	1.10	−0.60(10)
	1.25	−0.42(8)
	1.50	−0.01(5)
	1.75	0.64(14)
	1.85	0.92(5)
5[a]	0.90	−0.55(20)
	1.00	−0.15(21)
	1.10	0.12(13)
	1.25	0.73(25)

[a]The particulate–fluid interaction is of the type Lennard-Jones truncated at $r=3.8\sigma_f$.

obtained the contact angles of spherical substrates directly from the simulations following the methodology explained in Sec. II. Figure 5 depicts the contact angles as a function of the particulate–fluid interaction strength for several diameters: $\sigma_p/\sigma_f=5$, 7 and 10, and Table III presents the numerical data. For a given interaction strength an increase in the size of the particulate produces an increase in the contact angle, i.e., the particulate is pushed out from the liquid, or in other words becomes more ''hydrophobic''. This is a purely geometrical effect given that the interaction strength is constant. The geometrical effect includes changes in the curvature of the substrate and the volume excluded by the particulate. In particular the change in the curvature of the substrate affects the fluid–particulate surface tensions. The geometrical effect is more important in the neighborhood of the wetting transition (see Fig. 5), i.e., for large values of $\epsilon_{fp}/\epsilon_{ff}$. With regard to the drying transition the contact angles are essentially independent of the particulate size; that is, on the curvature of the substrate. As to the order of the transitions, our results suggest (see Fig. 5) that the wetting transition is first order, irrespective of the substrate curvature. Near the drying transition small particulates experience large fluctuations with respect to their equilibrium position. These small fluctuations can induce its detachment from the liquid–vapor interface and this precludes the measurement of the contact angles in the vicinity of the transition, and therefore the determination of the order. In any case for larger particulates ($\sigma_p/\sigma_f=10$) which are more stable at the interface, we do not find evidence of a second or weakly first order drying transition (see contact angles for $\sigma_p/\sigma_f=10$ in Fig. 5), in

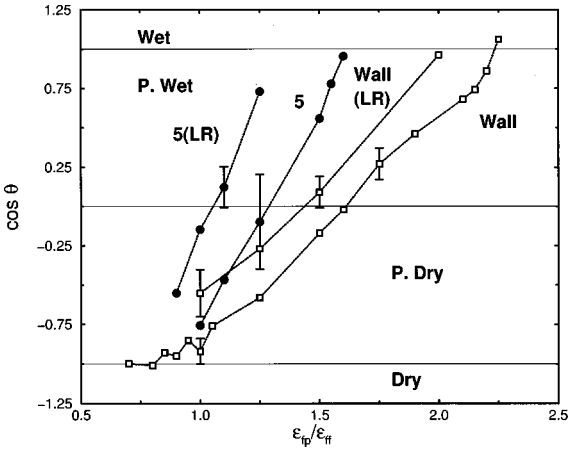

FIG. 6. Influence of the range of the particulate–fluid interaction on the contact angles as a function of particulate–fluid interaction strength for particulate size $5\sigma_f$, and the wall–fluid system. The legend LR refers to the results obtained using a Lennard-Jones potential with cutoff fixed at $3.8\sigma_f$. See Tables II and III for numerical values.

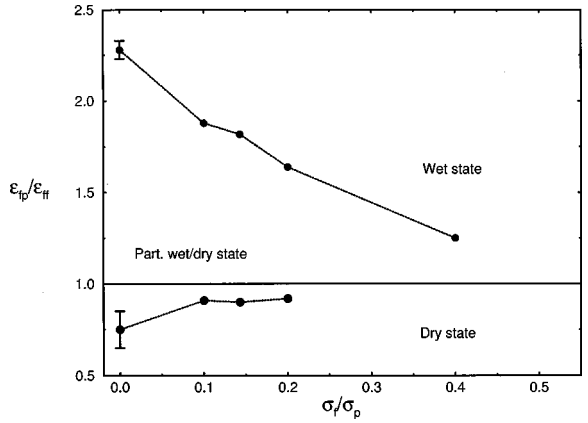

FIG. 7. Wetting–drying boundaries for the LJ/s model studied in this work.

contrast to the behavior observed in the wall–fluid system, i.e., for a particulate of infinite diameter.

In a recent study of wetting in a planar substrate, Bruin *et al.*[9] have analyzed the dependence of the order of the drying and wetting transitions with the substrate area. These authors observed that the order of the drying transition changes from a quasifirst order to a continuous transition with increasing substrate area, whereas the character of the wetting transition is not affected. Parry *et al.*[42] used a generalized Landau density–functional model to study the adsorption of a fluid at a nonplanar wall. These authors concluded that the roughness of the substrate can induce a change in the character of a wetting transition, from second to first order, even for small deviations from the plane. In our system the decrease in particulate size implies a decrease in the area of the substrate and an increasing deviation from planar geometry. Further work is required before we can ascertain whether there is a change in the order of the drying transition with the substrate size in our model.

In addition to geometrical effects it is expected that an increase in the range of the potential favors the wet state. To investigate this question we have considered a truncated LJ potential with the cutoff set to $3.8\sigma_f$, which is approximately twice as long as the range of the LJ/s potential $(1.737\sigma_f)$ considered above. In Fig. 6 we report results for a particulate of size $\sigma_p/\sigma_f=5$ and the planar limit. The increase in the range of the potential shifts the location of the wetting transition to smaller values of $\epsilon_{\rm fp}/\epsilon_{\rm ff}$, i.e., the contact angles decrease as the range of the potential increases. Thus as expected the wet state is favored. The drying transition is affected similarly. This result contrasts with the insensitivity of the drying transition to geometrical effects, as we have seen above. We have also analyzed the effect of the long range potential on the wall–fluid system. We observe similar trends to those seen in the particulate fluid case, and to those reported by Nijmeijer[43] in a study of a wall–fluid system. Again the contact angles decrease with the increase in the range of the potential, but these changes are somewhat smaller than those reported above for the particulate–fluid system (see Tables II and III and Fig. 6), suggesting that the combination of long range forces and curvature can act to enhance wetting to a greater extent than a change in the interaction by itself.

Figure 7 summarizes our results for the wetting properties of particulates at a liquid–vapor interface. We have represented the location of the wetting transition as a function of the particulate size σ_f/σ_p and the substrate–fluid interaction strength $\epsilon_{\rm fp}/\epsilon_{\rm ff}$. In order to calculate the wetting and drying transitions for the particulates we consider that the dependence of the contact angles with the interaction strength is linear. The intercept of these functions with the values $\cos\theta=-1$ and $\cos\theta=+1$ determine the drying and wetting transitions, respectively.

The wetting transition moves to smaller interaction strengths: $\epsilon_{\rm fp}/\epsilon_{\rm ff}$, as the particulate decreases its size. The precise location of the drying transition is subjected to some uncertainty as discussed above, nevertheless its dependence on particulate size seems to be very small as compared with the wetting transition. If we interpret the change in $\epsilon_{\rm fp}/\epsilon_{\rm ff}$ as a change in the temperature of the system, the diagram in Fig. 7 would indicate an increase of the wetting temperature as the particulate becomes smaller. This interpretation is in agreement with predictions from density functional theory concerning adsorption of fluids on colloidal particles.[13]

The shape of the diagram presented in Fig. 7 suggests that a change of the particulate size at constant $\epsilon_{\rm fp}/\epsilon_{\rm ff}$ does not produce a transition from a dry state to a wet state, but only from a wet to a partially wet state or from dry to a partially dry state. Thus the transition from a dry to a wet state can occur only by changing the substrate–fluid interaction strength, or in other words by changing the temperature. In addition we conclude that the partial dry and partial wet states disappear for small enough particulates, as indicated by the convergence of the wetting and drying boundaries represented in Fig. 7. Based on this behavior one can predict that small particulates are less stable in the interface than larger ones, given that a small change in the substrate fluid interaction strength $\epsilon_{\rm fp}/\epsilon_{\rm ff}$ or in other words, a small change in temperature due for instance to a thermal fluctuation, would push the particulate into the liquid or vapor phases. This observation agrees with the conclusions of Aveyard and

TABLE IV. Particulate–fluid surface tensions as a function of particulate size and interaction strength.

	$\epsilon_{fp}=1.25\epsilon_{ff}$			$\epsilon_{fp}=1.5\epsilon_{ff}$		$\epsilon_{fp}=1.75\epsilon_{ff}$	
σ_p/σ_f	γ^*_{pv}	$\gamma^{*\,a}_{pv}$	γ^*_{pl}	γ^*_{pv}	γ^*_{pl}	γ^*_{pv}	γ^*_{pl}
1	−0.072(8)	−0.079	−0.114(15)	−0.106(9)	−0.361(10)	−0.156(10)	−0.650(10)
2	−0.043(3)	−0.038	0.018(9)	−0.064(4)	−0.163(11)	−0.114(5)	−0.344(3)
3	−0.032(2)	−0.033	0.025(7)	−0.061(4)	−0.096(6)	−0.091(5)	−0.261(10)
4	−0.031(4)	−0.030	0.043(7)	−0.052(4)	−0.071(9)	−0.079(4)	−0.213(15)
5	−0.025(4)	−0.021	0.055(4)	−0.049(3)	−0.058(9)	−0.076(6)	−0.185(7)
7	−0.0245(10)	⋯	0.064(9)	−0.0457(10)	−0.043(4)	−0.069(3)	−0.152(5)
10	−0.025(3)	⋯	0.067(5)	−0.041(4)	−0.017(6)	−0.0661(10)	−0.1360(10)
∞	−0.0064(30)	⋯	0.090(7)	−0.024(6)	0.005(20)	−0.047(9)	−0.091(15)

[a]From Widom's insertion method (Ref. 44).

Clint[21] from a thermodynamic analysis of similar models.

For a particulate size $\sigma_p/\sigma_f=1$ and interaction strength $\epsilon_{fp}/\epsilon_{ff}=1$, the particulate becomes indistinguishable from the fluid particles. Given the vapor and liquid phases are in equilibrium and therefore the chemical potential is the same in both phases, the particle would be able to enter the liquid or vapor phase without restrictions, and therefore the drying/wetting transition would be undefined. Figure 7 is consistent with this limit, and it would be interesting to analyze in more detail how it is reached.

From Fig. 7 small particulates are more likely to be in a wet state than large particulates for similar substrate–fluid interaction strengths. Therefore small particulates exhibit enhanced solubility over larger ones. This situation can change, for instance, in the case of particulates with internal structure such as aggregates, where the change in particulate size might be accompanied by a change in the aggregate–fluid interaction strength. In any case our results suggest that geometrical factors play an important role in determining the solubility of the particulate in the liquid phase.

B. Analysis of the free energies: surface tension and line tension

The particulate–fluid surface tensions were computed using the methodology described in Sec. II comprising the simulation of a particulate immersed in the fluid at the liquid–vapor coexistence pressure (see Sec. II B for details). Table IV reports data for the particulate–fluid surface tensions for different particulate sizes, and Fig. 8 represents the liquid–particulate surface tensions as a function of the particulate size and the fluid–particulate interaction strength for two different choices of the surface of tension R_s (see Sec. II B for details on the surface of tension). In all these calculations we have considered the LJ/s potential to model the particulate–fluid interactions. The choice of the dividing surface appearing in Eq. (2.4) has an influence on the surface tension results. In our model the value $R_s=R$ produces surface tensions which are consistent, when extrapolated to the planar limit, with the surface tension of the wall–fluid system. If we consider $R_s=R+\sigma_f/2$ instead, the data are not consistent with this limit. We recall that the particulate–fluid surface tensions were calculated employing a thermodynamic route, whereas for the wall–fluid system we used the microscopic pressure tensor.

In Table IV we have included results for the particulate vapor surface tension obtained using Widom's[44] insertion method. This procedure allows the calculation of the absolute free energy of the particulate in the fluid, and along with Eq. (2.4) the surface tension. Both methodologies agree with each other for small particulates, up to $\sigma_p=5\sigma_f$. For larger particulates (not shown) Widom's method cannot be used due to the difficulty in inserting test particles.

Young's equation makes it possible to estimate the contact angle provided the surface tensions are known. It was pointed out in Sec. II that this equation is inaccurate when used to predict the contact angle of small spherical substrates. This is illustrated in Fig. 9, which represents the contact angles obtained both from Young's equation and direct observation as a function of the particulate size for different particulate–fluid interaction strengths. Young's equation becomes more inaccurate as the size of the particulate decreases, nonetheless for particulates on the order of $10\sigma_f$, it represents a good approximation. The discrepancies between the contact angles obtained from both routes can be explained in terms of the line tension which acts along the three phase line particulate/liquid/vapor. A decrease in the particulate size entails an increase in the curvature of the three phase line, the line tension has a larger influence, and therefore larger discrepancies with respect to the equilibrium con-

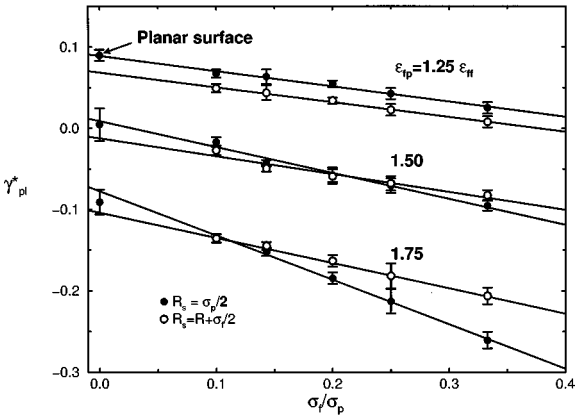

FIG. 8. Particulate–liquid surface tensions as a function of particulate size for different particulate–liquid interaction strengths. Black circles were obtained using $R_s=R$ as the surface of tension, and white circles with $R_s=R+\sigma_f/2$. The results for the wall–fluid system were obtained through the pressure tensor route.

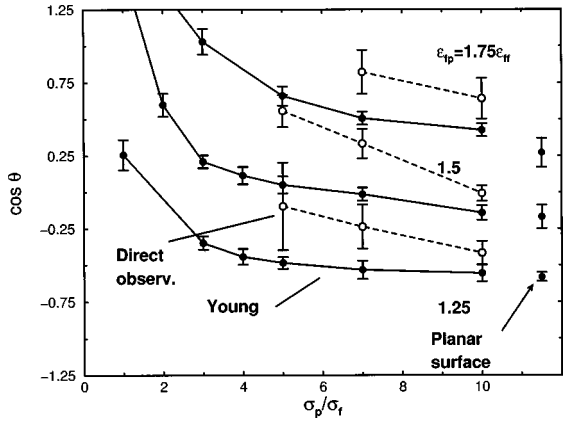

FIG. 9. Comparison of contact angles obtained through direct measurement (○) and from Young's equation (●), as a function of particulate size and fluid–particulate interaction strength.

tact angles should be observed, as seen in Fig. 9. The effect of the line tension on the contact angle can be summarized in a corrected Young's equation:

$$\gamma_{pv}-\gamma_{pl}-\gamma_{lv}\cos\theta+\frac{\tau\cos\theta}{R\sin\theta}=0, \tag{3.2}$$

which results from considering the balance of the forces operating in the system represented in Fig. 1. Alternatively Eq. (3.2) can be obtained by minimizing expression (2.3) with respect to the contact angle, considering the surface and line tensions independent of the angle.

The computation of the line tension was performed using the methodology introduced by us previously[36] and explained in Sec. II B. As in the case of the surface tensions discussed above, we have considered the LJ/s potential to model the fluid–particulate interactions. Provided the particulate is at the liquid/vapor interface, the procedure involves the computation of the work needed to increase/decrease the radius of the particulate by a certain amount ΔR. We relate this work with the free energy given in expression (2.10), which can be calculated in the canonical ensemble employing Eq. (2.5) as explained in Sec. II. Alternatively one can estimate the line tension using the balance equation [Eq. (3.2)]. This route has the advantage that it only requires the surface tensions and the contact angles for a given particulate radius. Given that Eq. (3.2) corresponds to the derivative of the free energy of the particulate at the interface F^s, with respect to the contact angle, it follows that for a given line tension the contact angle in the expression, Eq. (3.2), is such that F^s presents an extrema, i.e., a maximum or a minimum. The equilibrium contact angle corresponds to a minimum in the free energy. As a third approach to the computation of the line tension we consider Eqs. (2.10) and (3.2); from the free energy and surface tensions it is possible to get both the contact angle that minimizes the free energy and the line tension.

As pointed out elsewhere,[21] the solutions of Eqs. (2.3) and (3.2) may correspond either to stable, metastable, or unstable states. We are interested in the values of contact angles and line tensions which correspond to a stable situation. The instability boundaries that follow from Eqs. (2.3) and (3.2) can be determined by considering the following values for the contact angles:[21]

TABLE V. Comparison of the contact angles measured directly, cos θ, with the angles, cos θ_u and cos θ, which determine unstable and metastable states using Eqs. (2.3) and (3.2).

$\epsilon_{fp}/\epsilon_{ff}$	σ_p/σ_f	cos θ_0	cos θ_u	cos θ_t	cos θ
	5.0	−0.48	−0.78	−0.60	−0.10(33)
1.25	7.0	−0.53	−0.81	−0.64	−0.24(15)
	10.0	−0.56	−0.82	−0.67	−0.42(8)
	5.0	0.05	0.37	0.09	0.56(11)
1.5	7.0	−0.02	−0.27	−0.04	0.33(10)
	10.0	−0.14	−0.52	−0.23	−0.01(5)
1.75	7.0	0.51	0.80	0.63	0.82(15)
	10.0	0.42	0.75	0.54	0.64(14)

$$\cos\theta_u=(\cos\theta_0)^{1/3}, \tag{3.3}$$

where cos θ_0 represents the contact angle obtained from Young's equation. Let us consider first the case $\theta_0<90°$; for cos $\theta<$cos θ_u the particulate is not stable at the interface. For $\theta_0>90°$ the instability appears when cos $\theta>$cos θ_u (see Ref. 21 for a further discussion of these conditions). As pointed out by Aveyard and Clint[21] there is another set of angles for which the particulate experiences a wetting or a drying transition. These angles can be obtained from the relation:[21]

$$\cos\theta_0=0.5\cos\theta_t(1\pm\cos\theta_t), \tag{3.4}$$

where the plus sign refers to $\theta_0<90°$ and the minus sign to $\theta_0>90°$. Therefore for $\theta_0>90°$ and cos $\theta_u>$cos $\theta>$cos θ_t the particulate would be in a metastable state. In the same way for $\theta_0<90°$ this state would appear when cos $\theta_t<$cos $\theta<$cos θ_u. Otherwise the stable states are those which fulfill the condition cos $\theta>$cos θ_t ($\theta_0<90°$) and cos $\theta<$cos θ_t ($\theta>90°$).

We have explored the stability of the states considered in our work by applying the conditions introduced above. In Table V we compare the contact angles measured directly during the simulation cos θ with the values cos θ_u and cos θ_t introduced previously. Interestingly some of the states we have simulated, cf. $(\epsilon_{fp}/\epsilon_{ff},\sigma_p/\sigma_f)=(1.5,5)$, (1.75,7), which correspond to the partially wet regime, are in the unstable region as given by Eqs. (2.3) and (3.2), whereas other states [cf. (1.75,10)] are metastable. In spite of this during the long runs we performed for these states (5×10^5 time steps) we did not observe any indication of instability. It may be that the equilibration time required by the system to attain the equilibrium contact angle is much longer than the length of the trajectories considered here. If that were the case a relatively small modification of the contact angle could change the character of some states which now appear to be unstable or metastable [see for instance data of the contact angles for the states (1.75,7) and (1.75,10)]. Longer runs are then necessary to ascertain whether there is insufficient equilibration of the simulations used for the calculation of

TABLE VI. Results for the line tension, $\tau^* = \tau\sigma_f/\epsilon_{ff}$, and contact angles as a function of fluid–particulate interaction strength and particulate size. The fluid–particulate interaction is of the LJ/s type.

$\epsilon_{fp}/\epsilon_{ff}$	σ_p/σ_f	τ^{*a}	τ^{*b}	τ^{*c}	$\cos\theta^{d}$	$\cos\theta^{b}$	$\cos\theta^{e}$
	5.0	−0.22	−0.18	−1.58	−0.10	−0.33	−0.48
1.25	7.0	−0.29	−0.26	−0.69	−0.24	−0.36	−0.53
	10.0	−0.18	−0.18	−0.25	−0.42	−0.45	−0.56
1.50	10.0	−0.30	−0.25	−11.0	−0.01	−0.11	−0.14
	10.0[f]	−0.20	−0.20	−12.5	−0.01	−0.10	−0.12

[a]From Eq. (2.10).
[b]From Eqs. (2.10) and (3.2).
[c]From Eq. (3.2).
[d]From direct observation.
[e]From Young's equation.
[f]Using $R+\sigma_f/2$ instead of R.

the contact angles or that Eqs. (2.3) and (3.2), which are after all macroscopic expressions, do not adequately represent the wetting behavior of these particulates.

From the discussion above, in order to use Eqs. (2.3) and (3.2) to estimate the line tensions, the states considered should correspond to stable cases. Otherwise the use of these equations can produce line tensions and contact angles which are inconsistent. Data for the line tensions and contact angles of the stable states are presented in Table VI. The three routes described above to estimate the line tension produce similar results in magnitude and sign. Nonetheless the balance equation has a divergence at $\cos\theta=0$. This influences the accuracy of the line tensions that can be estimated from this route, as seen for instance in the states $\sigma_p/\sigma_f=5$, $\epsilon_{fp}/\epsilon_{ff}=1.25$, and $\sigma_p/\sigma_f=10$, $\epsilon_{fp}/\epsilon_{ff}=1.5$. The current results for the interaction strength $\epsilon_{fp}/\epsilon_{ff}=1.25$ agree well with the data published previously.[36] The line tensions are independent of the particulate size and apparently on the interaction strength, although more data would be necessary to confirm this statement.

The calculation of the line tensions through expressions (2.10) and (3.2) depends, as in the case of the surface tensions, on the choice of the radius R, which defines the surface of tension. We have analyzed the effect of the value of this radius on the line tension. In Table VI we have included a representative case using $R+\sigma_f/2$ instead of R. We employed the surface tensions consistent with this choice of the surface of tension. The new results do not alter significantly the value of the line tension with respect to the previous data.

As discussed in a previous publication,[36] the line tensions for our system are of the order[45] $\approx 10^{-12}$ N, which is one order of magnitude smaller than values reported for overbased detergents at the water–air interface.[16] This difference might well be due to the larger surface tension of the water–air interface, $\gamma=0.072$ N/m, as compared with the liquid–vapor interface considered here, $\gamma=0.003$ N/m.

IV. SUMMARY AND CONCLUSIONS

In this work we have analyzed the wetting behavior of spherical particulates at a liquid/vapor interface. The model potential considered for the particulate–fluid interaction was chosen such that it is independent of the size of the particulate, even for a particulate of infinite radius. In this case the model we have studied is equivalent to a liquid in equilibrium with its vapor, in the presence of a planar structureless substrate.

We have analyzed the wetting and drying behavior of the particulate as a function of size, fluid–particulate interaction strength, and potential range. Our study is focused mainly on the properties of particulates with sizes on the nanometer scale, but in order to compare the results with a planar surface we considered as well the case of a wall–fluid system. For a given particulate–fluid interaction strength the contact angle increases with the size of the particulate, i.e., the particulate becomes more ''hydrophobic.'' This behavior is due solely to geometrical effects. Our conclusions (see Fig. 7) can be summarized as follows: (1) The wetting transition shifts to smaller particulate–fluid interaction strengths as the particulate becomes smaller, whereas the drying transition has a very weak dependence on particulate size. (2) The transition from a dry to a wet state can occur only by changing the particulate–fluid interaction strength. An increase or decrease of the size of the particulate at fixed interaction strength results only in a transition from a wet/dry state to a partially wet/partially dry one, respectively. (3) Small particulates are less stable at the liquid–vapor interface than large ones. Thus small thermal fluctuations can, in principle, push the particle into one of the phases: liquid or vapor. This result agrees with previous theoretical studies of similar systems using thermodynamic analysis. (4) Given that for fixed interaction strength the wetting state is favored as the particulate becomes smaller, our results suggest that a change in the geometry of the particulate can enhance its solubility.

With regard to the possible order of the wetting and drying transitions, the wetting transition is first order in agreement with previous observations in wall–fluid systems. A change in the particulate size or, in other words, in the substrate curvature does not alter this behavior. With regard to the drying transition the order is not so well defined. For a wall–fluid system we obtain results compatible with a second or weakly first order transition. For small spherical particulates it is not easy to determine accurately the behavior of the contact angles in the neighborhood of the drying transition, and this fact precludes the determination of the order.

Real substrates contain imperfections, i.e., a certain de-

gree of roughness. Our work suggest that a curved surface can be wetted more easily than a planar surface provided the fluid–substrate interaction strength is essentially the same. Theoretical studies suggest that the roughness of the substrate plays an important role in the modification of the wetting properties of the system, and indeed can enhance wetting.[42,46,47] From experiment it is also known that surface roughness enhances wetting.[48] Recently Tang and Harris[8] have studied by molecular dynamics simulation the effect of roughness on the wetting transition, considering surface vacancies in a wall with structure. These authors observe that the wetting properties are very sensitive to the detailed molecular structure of the surfaces. In their model the wetting is easier on a planar substrate than on the rough surface. These results contrast with the common belief that roughness enhances wetting. From our model we can conclude that the wetting properties are indeed very sensitive to both geometry and interaction strength, and even though a change in geometry can enhance wetting, this enhancement could be compensated by an analogous change in the substrate–fluid interaction strength.

We have analyzed the effect of the range of the interactions on the wetting behavior of our model. An increase in the range of the potential favors wetting. These changes affect almost to the same extent the wetting and the drying transitions. Interestingly the modification of the contact angles due to an increase in the range of the substrate–fluid interactions is larger in curved surfaces than in planar substrates.

In order to calculate the fluid–particulate surface tensions we have employed a thermodynamic approach proposed in a previous article.[36] The calculation of the surface tension requires the choice of the surface of tension R_s. We have analyzed the effect of varying R_s on the surface tensions, and we find that the choice $R_s=R$ gives surface tensions which are consistent with the values obtained for a planar surface. The latter were calculated using a microscopic route, i.e., by evaluating the pressure tensor. We have used these values of the surface tensions to test the accuracy of the Young's equation in the prediction of the wetting properties of particulates at a liquid–vapor interface. For small particulates Young's equation predicts contact angles which differ significantly from the angles measured directly during the computer simulation. The differences decrease as the particulate size increases and for the larger sizes considered in this work ($\sigma_p/\sigma_f=10$) Young's equation represents a reasonable approximation for the contact angles. This is probably related to the magnitude of the line tension in our system, which would have a small influence on the contact angles for the larger particulates considered in this work.

We have estimated the line tension of our model employing three different routes. The first route uses Eq. (2.10), and requires a knowledge of the contact angles, surface tensions, and free energy of the particulate at the interface. A second route is based on the solution of the balance Eq. (3.2), and requires the surface tensions and the contact angles. Finally the third route involves the solution of Eqs. (2.10) and (3.2), giving the line tension and contact angles from the free energy and surface tensions. In order to obtain consistent results we have calculated the line tensions only for those states which correspond to stable solutions of these equations. Additional simulations are required to determine whether Eqs. (2.3) and (3.2) are accurate for all the present systems and therefore particulates which correspond to unstable solutions become unstable in larger simulations, or alternatively that the contact angles measured in this work correspond to equilibrium states, and Eqs. (2.3) and (3.2) break down for some cases.

We have estimated the line tensions for the states which correspond to stable solutions of Eqs. (2.3) and (3.2). The line tensions for our system are negative and their magnitudes do not show a clear dependence on particulate size or interaction strength. The line tension, $\approx 10^{-12}$ N, is one order of magnitude smaller than that observed in real systems which involve colloidal particles at a water/air interface. We believe that this difference might be due to the smaller surface tension of the interface considered in this work as compared with the water/air interface.

ACKNOWLEDGMENT

The authors acknowledge the award of EPSRC Research Grant No. GR/L 51997.

[1] E. M. Blokhuis and B. Widom, Curr. Opin. Colloid Interface Sci. **1**, 424 (1996), and references therein.
[2] J. H. Sikkenk, J. O. Indekeu, J. M. J. van Leeuwen, E. O. Vossnack, and A. F. Bakker, J. Stat. Phys. **52**, 23 (1988).
[3] M. J. P. Nijmeijer, C. Bruin, A. F. Bakker, and J. M. J. van Leeuwen, Physica A **160**, 166 (1989).
[4] M. J. P. Nijmeijer, C. Bruin, A. F. Bakker, and J. M. J. van Leeuwen, Phys. Rev. A **42**, 6052 (1990).
[5] M. J. P. Nijmeijer, C. Bruin, A. F. Bakker, and J. M. J. van Leeuwen, Phys. Rev. B **44**, 834 (1991).
[6] J. Hautman and M. L. Klein, Phys. Rev. Lett. **67**, 1763 (1991).
[7] C. F. Fan and T. Cagin, J. Chem. Phys. **103**, 9053 (1995).
[8] J. Z. Tang and J. G. Harris, J. Chem. Phys. **103**, 8201 (1995).
[9] C. Bruin, M. J. P. Nijmeijer, and R. M. Crevecoeur, J. Chem. Phys. **102**, 7622 (1995).
[10] N. S. Desai and C. Franck, Phys. Rev. E **50**, 429 (1994).
[11] J. R. Henderson, P. Tarazona, F. van Swol, and E. Velasco, J. Chem. Phys. **96**, 4653 (1992).
[12] R. Defay, I. Prigogine, A. Bellemans, and D. H. Everett, *Surface Tension and Adsorption* (Longman and Green, London, 1966), pp. 310–348.
[13] D. Henderson, S. Sokolowski, and A. Patrykiejew, Mol. Phys. **85**, 745 (1995).
[14] I. Hadjiagapiou, J. Chem. Phys. **105**, 2927 (1996).
[15] H. Löwen, Z. Phys. B **97**, 269 (1995).
[16] R. Aveyard and J. H. Clint, J. Chem. Soc., Faraday Trans. **91**, 2681 (1995).
[17] J. A. Griffiths, R. Bolton, D. M. Heyes, J. H. Clint, and S. E. Taylor, J. Chem. Soc., Faraday Trans. **91**, 687 (1995).
[18] J. S. Rowlinson and B. Widom, *Molecular Theory of Capillarity* (Oxford Science, 1989).
[19] J. O. Indekeu, Int. J. Mod. Phys. B **8**, 309 (1994).
[20] B. Widom, J. Phys. Chem. **99**, 2803 (1995).
[21] R. Aveyard and J. H. Clint, J. Chem. Soc., Faraday Trans. **92**, 85 (1996); *ibid.* **92**, 4271 (1996).
[22] B. A. Pethica, J. Colloid Interface Sci. **62**, 567 (1977).
[23] L. Boruvka and A. W. Neumann, J. Chem. Phys. **66**, 5464 (1977).
[24] G. Navascués and P. Tarazona, J. Chem. Phys. **75**, 2441 (1981).
[25] P. G. de Gennes, Rev. Mod. Phys. **57**, 827 (1985).
[26] B. M. Law, Phys. Rev. Lett. **69**, 1781 (1992).
[27] V. Talanquer and D. W. Oxtoby, J. Chem. Phys. **104**, 1483 (1996).
[28] T. Getta and S. Dietrich, Phys. Rev. E **57**, 655 (1998).
[29] J. Drelich, Colloids Surf., A **116**, 43 (1996).

[30] A. Scheludko, B. V. Toshev, and D. T. Bojadjiev, J. Chem. Soc., Faraday Trans. 1 **72**, 2815 (1976).
[31] J. Mingins and A. Scheludko, J. Chem. Soc., Faraday Trans. 1 **75**, 1 (1979).
[32] P. A. Kralchevsky, A. D. Nikolov, and I. B. Ivonov, J. Colloid Interface Sci. **112**, 132 (1986).
[33] J. Drelich and J. D. Miller, J. Colloid Interface Sci. **164**, 252 (1994).
[34] D. Duncan, D. Li, J. Gaydos, and A. W. Neumann, J. Colloid Interface Sci. **169**, 256 (1995).
[35] T. Pompe, A. Fery, and S. Herminghaus (private communication, 1998).
[36] F. Bresme and N. Quirke, Phys. Rev. Lett. **80**, 3791 (1998).
[37] B. L. Holian and D. J. Evans, J. Chem. Phys. **78**, 5147 (1983).
[38] W. G. Hoover, *Computational Statistical Mechanics* (Elsevier, Amsterdam, 1991).
[39] J. M. Hayle, *Molecular Dynamics Simulation: Elementary Methods* (Wiley, New York, 1992).
[40] M. P. Allen and D. J. Tildesley, *Computer Simulation of Liquids* (Clarendon, Oxford, 1987).
[41] E. Velasco and P. Tarazona, J. Chem. Phys. **91**, 7916 (1989).
[42] A. O. Parry, P. S. Swain, and J. A. Fox, J. Phys.: Condens. Matter **8**, L659 (1996).
[43] M. J. P. Nijmeijer, Ph.D. thesis, Rijksuniversiteit te Leiden, 1990.
[44] B. Widom, J. Chem. Phys. **39**, 2808 (1963).
[45] We have considered the parameters $\sigma_p = 3.4$ Å, $\epsilon_{\mathrm{ff}}/k_B = 166$ K, as representative of argon. The value for $\epsilon_{\mathrm{ff}}/k_B$ is based on the critical temperature of the LJ/s potential $T_c^* = 0.91$.
[46] C. Borgs, J. de Coninck, R. Kotecký, and M. Zinque, Phys. Rev. Lett. **74**, 2292 (1995).
[47] R. R. Netz and D. Andelman, Phys. Rev. E **55**, 687 (1997).
[48] R. N. Wenzel, J. Phys. Colloid Chem. **53**, 1466 (1949); R. N. Wenzel, Ind. Eng. Chem. **28**, 988 (1936).